Simulation-Based Study of Propulsion and Control of an AUV in Current-Affected Environments

Aymen Mefti, Mahfoudh Cerdoun
Ecole Militaire Polytechniques
Alger, Algeria
email: aymen21mefti@gmail.com
email: cerdoun.mahfoudh@gmail.com

Djahida Boucetta
Royal Military Academy RMA
Brussel, Belgium
email: djahida.boucetta@mil.be

Abstract— **This study presents a numerical investigation into the hydrodynamic behavior and control of an Autonomous Underwater Vehicle (AUV) operating in current-affected marine environments. Initially, a self-propulsion test has been conducted to determine the optimal propeller rotational speed required to overcome the AUV's hydrodynamic resistance during a steady, straight-line motion. Subsequently, the effect of the lateral marine current has been examined, introducing additional transverse resistance that require dynamic adjustments in both rudder deflection and propeller rotational speed to keep a fixed forward speed. Therefore, a parametric analysis of the AUV's response to varying control configurations is investigated, focusing on the effects of rudder deflection angles and propeller rotational speeds on the surge, sway, and yaw motion. The overall numerical approach is validated using the propeller open water experimental data. The results highlight the effectiveness of coupled hydrodynamic simulation and control input strategies in predicting and managing AUV behavior in complex and dynamic marine environments.**

Keywords-Autonomous Underwater Vehicle (AUV); Self propulsion; Marine Currents; Hydrodynamic Simulation; Propeller Performance.

I. INTRODUCTION

Autonomous Underwater Vehicles (AUVs) have become indispensable tools across a broad spectrum of scientific and industrial domains. Their deployment enables operations that are hazardous, impractical, or impossible for human divers, particularly in deep-sea exploration where AUVs facilitate the discovery and detailed mapping of previously inaccessible marine environments [1]. Beyond exploration, AUVs play a crucial role in conducting oceanographic experiments, performing seabed surveys for geological and geographical research, and acquiring high-resolution data in real time [2]. In response to these growing demands, considerable research efforts have been directed toward enhancing the hydrodynamic efficiency and autonomous capabilities of AUVs. A key challenge lies in comprehensively understanding the complex fluid dynamics around AUVs, which is complicated by the presence of multiple interacting components such as propellers, rudders, and control fins [3].

Moreover, the remote and often prolonged nature of AUV missions imposes stringent requirements on autonomy and control systems. AUVs must operate independently in dynamic and often unpredictable underwater environments, necessitating sophisticated control algorithms, robust navigation systems, and efficient energy management strategies to maximize operational range and mission duration [4] [5].

The AUVs have attracted considerable research interest. Honaryar and Ghiasi [6] introduced a bio-inspired hull design modeled after the catfish *Hypostomus*. Based on numerical simulations and experimental studies, they demonstrated an approximately 99% improvement in the hydrodynamic stability. Yu et al. [7] investigated the Underwater Radiated Noise (URN) through a coupling of Computational Fluid Dynamics (CFD) with Lighthill's acoustic analogy, and these investigations allow identification of cavitation and propeller vibrations as principal noise sources. Similarly, Wu et al. [8] performed physics-based simulations of a free-running propeller-driven AUV. The results revealed transient thrust fluctuations and wake structures that are critical for understanding propulsion efficiency. Environmental interactions, such as wave-current coupling, further complicate AUV performance [9]-[14]. Ding et al. [9] numerically analyzed the DARPA Suboff submarine with a pump-jet propulsor operating near the free surface. Min et al. [10] introduced a hybrid CFD and system identification approach to model multi-propeller AUV maneuvering, enabling accurate extraction of hydrodynamic parameters for control system design. Raja et al. [11] explored unmanned amphibious systems integrating aerial and marine domains via multi-domain simulations, highlighting innovative propulsion and control strategies for enhanced marine surveillance capabilities. The effects of control surface deflections and hydrodynamic interactions among multiple AUVs have also been extensively studied. Dantas and de Barros [12] employed Reynolds-Averaged Navier-Stokes (RANS) CFD to capture nonlinear hydrodynamic forces on hulls and control surfaces, whereas Rattanasiri et al. [13] and Hong et al. [14] analyzed hydrodynamic interactions within tandem AUV formations.

Further studies have examined propeller-induced interactions and wave effects [15]-[21]. Liu et al. [15] reported thrust enhancements of up to 7% for two propeller-

driven Unmanned Underwater Vehicles (UUVs) in formation. Tian et al. [16] employed two-phase CFD to analyze wave impacts on an axisymmetric AUV near the surface, revealing lift and drag sensitivity to wave parameters. Liu et al. [17] numerically evaluated the UUV's hydrodynamics and self-propulsion near the seabed.

Despite the extensive literature concerning the hydrodynamics of AUVs, a significant research gap persists in thoroughly examining the coupled effects of propulsion and stability under time-varying marine currents. Previous studies have primarily addressed individual aspects such as hull design, propeller performance, or specific environmental interactions. However, the combined influence of lateral current forces on AUV propulsion and trajectory stability has not been systematically investigated using high-fidelity numerical simulations. This omission is critical, as lateral currents can substantially modify hydrodynamic loads, induce yaw or drift, and ultimately degrade navigational accuracy.

The present study attempts to fill this gap by conducting a simulation-based investigation of AUV propulsion and stability in current-affected environments. Employing RANS modeling, the work quantifies hydrodynamic responses and assesses how lateral disturbances impact straight-line motion. By providing detailed insights into the coupled behavior of the AUV and its operational environment, this research contributes to an integrated understanding of AUV performance under realistic marine conditions.

The remainder of this paper is organized as follows. Section II provides a detailed description of the numerical modeling framework, including the AUV geometry, computational domain and boundary conditions, mesh configuration, and the numerical procedure. Section III presents the validation of the simulation methodology against experimental propeller data. Section IV discusses the results, while Section V concludes the study and outlines directions for future work.

II. NUMERICAL MODELLING

The numerical simulations conducted in this study—both for the self-propulsion analysis and for the AUV operating under current-affected conditions—were performed using the commercial CFD software ANSYS CFX [18]. Coupling with MATLAB was employed to support parameter control and data processing. This section provides a detailed description of the AUV's geometric components, including the hull, rudders, and propeller, as well as the numerical setup and modeling approach

A. AUV Geometry

The full scale self-propelled AUV utilized in this study consists of three main components: the hull, the finned rudder plates, and the propeller, as illustrated in Figure 1. The shapes of the nose and tail sections are determined from [19], L_h, L_c and L_c are the lengths of nose, body and tail sections, respectively. D_A is the maximum diameter, n is an exponential parameter which can be varied to give different body shapes ($n = 1.8$ in the current study), and θ is the included angle at the tip of the tail. The total length of the AUV is 2 meters. Detailed dimensional parameters are provided in Table 1.

The rudder blades (Figure 2) employ a flat-plate airfoil profile, characterized by a circular leading edge that has a radius of 4 mm and a trailing edge with a radius of 1.6 mm. The trailing edge of every rudder blade is positioned 1925 mm from the nose of the AUV. The chord length of the blade varies linearly across the span, starting at 82 mm at the hub and tapering down to 7 mm at the tip. The DTMB 4119 model propeller (Figure 3) has been selected to propel the vehicle. Its specific geometric details are presented in Table 2.

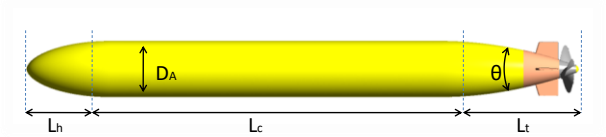

Figure 1. The AUV Geometry.

TABLE 1. MAIN PARAMETERS OF AUV HULL.

Parameters	Value
D_A	0.2 m
L_A	2m
L_h	0.3m
L_c	1.2m
L_t	0.5m
θ	20°

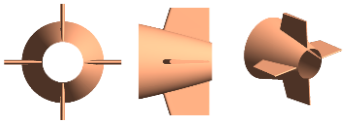

Figure 2. The Rudder Geometry.

TABLE 2. DETAILED PARAMETERS OF THE DTMB 4119 PROPELLER.

D(m)	0.1829
Z	3
Skew(°)	0
Rake(°)	0
Blade section	NACA 66 a=0.8
Rotation direction	Right

Figure 3. The DTMB 4119 Marine Propeller.

B. Computational domain and Boundary conditions

The computational domain (Figure 4) consists of a cylindrical volume that surrounds the AUV. Its dimensions are selected to reduce the influence of boundary effects on the flow field solution: the domain extends a distance of L_A upstream from the inlet, $3L_A$ downstream from the outlet,

and *10*D_A in the radial direction outwards the far field, where L_A is the length of the AUV is and D_A is its diameter. To accurately capture the complex flow patterns near the propeller, the computational domain is segmented into two subdomains: One that rotates around the propeller and another that remains stationary, representing the outer flow domain. The flow around the propeller is modeled using a Moving Reference Frame (MRF) approach within the rotating region. The interface between the rotating and stationary subdomains is handled using a General Grid Interface (GGI) with a "frozen rotor" condition, which facilitates the transfer of flow variables and guarantees precise coupling between the two regions while maintaining stable and realistic flow dynamics.

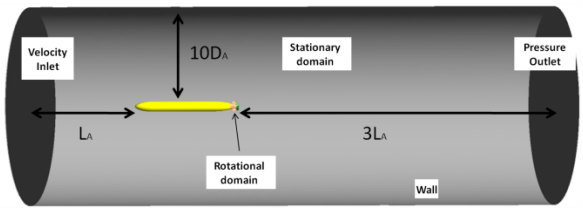

Figure 4. Computational domain with boundary conditions.

The boundary conditions were defined as presented in Figure 4. A no-slip wall condition was applied on the hull, rudder, and propeller surfaces. The propeller was modeled as a rotating wall. The presence of a lateral marine current introduces an additional velocity component, $V_{current}$, (Figure 5) which introduces additional hydrodynamic loads on the AUV. To maintain the desired forward speed and trajectory, it becomes necessary to adjust the rudder blade orientation angles and the propeller rotation speed accordingly. This control strategy forms the focus of the second part of our study.

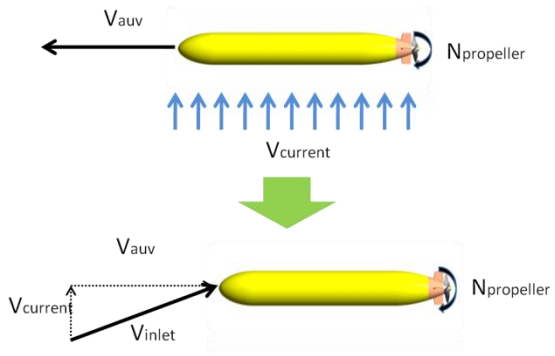

Figure 5. Modeling of the Effect of Lateral Marine Currents.

To account for the effect of the lateral marine current, the computational domain was modified by rotating the AUV about the *z*-axis by an angle $\alpha_{current}$, defined as $\alpha_{current} = \tan^{-1}(V_{current}/V_{auv})$. Additionally, the inlet velocity was updated to incorporate both the AUV's advance speed and the current velocity, as illustrated in Figure 5. Figure 6 presents the modified computational domain used in the second part of this study.

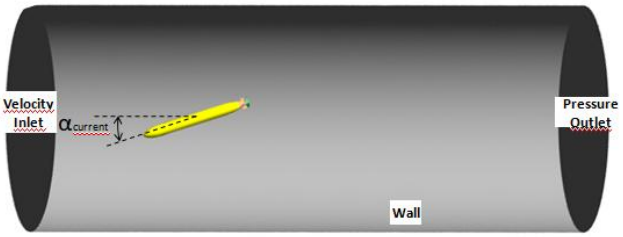

Figure 6. Computational domain considering the effect of lateral marine current.

C. *Mesh Setup*

A hybrid mesh was employed for the computational domain, consisting of structured elements around the propeller and rudder, and unstructured elements for the hull. Structured elements were also applied within the boundary layer regions surrounding the hull, propeller, and rudder to accurately capture near-wall effects. Additionally, local mesh refinement was implemented in regions with abrupt geometric changes, Such as the leading and trailing edges, as shown in figure 7. The computational domain consists of approximately 9 million elements, of which about 3 million belong to the rotary domain and 6 million to the stationary domain.

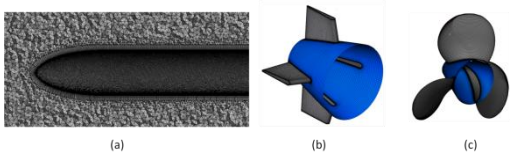

Figure 7. Surface Mesh: - (a) Hull - (b) Rudder - (c) Propeller.

D. *Numerical Procedure*

The self-propulsion point of the AUV, in straight-line mode, is defined as a combination of AUV constant speed and propeller Revolutions Per Minute (RPM) rate in which the propeller thrust force matches AUV hydrodynamic resistance. This resistance arises from various components, including the hull, control surfaces, such as rudders, and external appendages like sensors. From a mathematical standpoint, this condition corresponds to the propeller rotational rate at which the net force on the vehicle vanishes, consistent with Newton's second law (1).

$$T + R_{hull} + R_{ruddder} = 0 \quad (1)$$

Here, T denotes the thrust generated by the propeller, while R_{hull} and R_{rudder} represent the hydrodynamic resistance of the hull and rudder, respectively. The procedure to determine the self-propulsion condition is based on an iterative process in which a numerical simulation is performed at each iteration. Once the simulation converges,

the relevant hydrodynamic forces are extracted through post-processing. These values are then used to evaluate (1), which serves as the convergence criterion. Based on the obtained results, the propeller's rotational velocity is updated using the secant method (2). This process is repeated iteratively until the self-propulsion condition is satisfied.

$$\begin{cases} N_{i+1} = N_i - F_i \times \frac{N_i - N_{i-1}}{F_i - F_{i-1}} \\ F_i = T_i + R_{hull_i} + R_{rudder_i} \end{cases} \quad (2)$$

When an AUV traveling along a straight path at steady speed encounters a current-affected environment with lateral flow (Figure 8), it experiences additional hydrodynamic forces. These forces induce sway and yaw motions, causing the vehicle to deviate from the intended trajectory and potentially compromising its directional stability. In the absence of corrective control actions, the AUV will drift and may gradually veer off from its original heading. Consequently, active control systems are essential for preserving trajectory and heading stability under such flow-disturbed conditions.

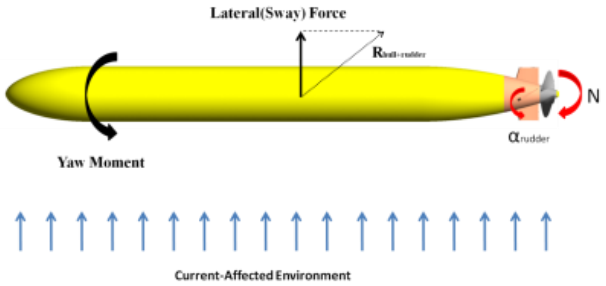

Figure 8. Effect of Cross-Current on AUV Stability and Trajectory.

A series of numerical simulations was conducted to assess the AUV's response to lateral current disturbances while implementing different corrective control measures. In particular, two control parameters were investigated: the deflection angle of the upper and lower rudder blades, referred to as α_{rudder} throughout this study, and the rotational propeller rate, denoted as *N(rpm)*.

III. VALIDATION

To validate the numerical methodology, the hydrodynamic performance of the E779A marine propeller is evaluated through numerical simulations. This specific propeller has been extensively investigated both numerically and experimentally in the literature [20] [21]. Simulations were performed to compute the open water characteristics, which are then compared with the experimental data available in [20]. The open water characteristics illustrate the propeller's performance in a uniform flow field, and are expressed using several key dimensionless parameters: the advance coefficient J, the thrust coefficient K_T, the torque coefficient K_Q, and the open water efficiency η. During the simulations, the rotational speed is maintained at a constant value of 11.7881 rps, while the inflow velocity is varied to alter the advance coefficient J and three operating conditions were tested. The comparison of the numerical results to the experimental data for thrust and torque coefficients is summarized in Table 3.

TABLE 3. COMPARISON OF THRUST AND TORQUE COEFFICIENTS UNDER NON-CAVITATING OPEN-WATER CONDITIONS.

J	$K_{T_{NUM}}$	$10K_{Q_{NUM}}$	$er_{K_T}(\%)$	$er_{K_Q}(\%)$
0.348	0.409	0.685	0.362	1.587
0.747	0.217	0.413	-2.118	1.99
0.946	0.119	0.267	-5.17	4.871

The deviations in thrust and torque coefficients range from 0.36% to 5.17%, indicating a significant level of concordance with experimental data and affirming the model's validity under open-water conditions.

IV. RESULTS AND DISCUSSION

A. *Self-Propelled AUV*

The initial study aims to determine the self-propulsion condition of the Autonomous Underwater Vehicle (AUV) described above. This is achieved using a Computational Fluid Dynamics (CFD) approach based on RANS equations, in conjunction with a MATLAB script, following the computational procedure outlined in Figure 9. The AUV is assumed to travel in a straight trajectory at a steady speed of 5 m/s. The self-propulsion condition is obtained using the secant method, which requires two initial estimates for the propeller rotational speed, denoted as N0 and N1. These initial speeds are established at 1400 rpm and 1500 rpm, respectively. The convergence criterion is defined as $e = \frac{|F|}{T} < 0.001$, where F represents the residual force and T is the thrust, ensuring that the solution reaches an acceptable level of accuracy.

Figure 9 illustrates the behavior of the Secant method during the numerical assessment of the self-propulsion condition. In Figure 9(a), the normalized residual force, is plotted against the iteration number to assess convergence. The method required a total of six iterations, including the two initial guesses, to reach convergence. Figure 9(b) depicts the residual force F(N) as a function of the propeller rotational speed N. The red markers trace the sequence of estimates generated by the Secant method, clearly indicating convergence toward the zero-residual point. The dashed horizontal line at F(N)=0 represents the condition of exact thrust-resistance equilibrium. The intersection confirms that the propeller generates

exactly the thrust required to overcome the vehicle's hydrodynamic resistance.

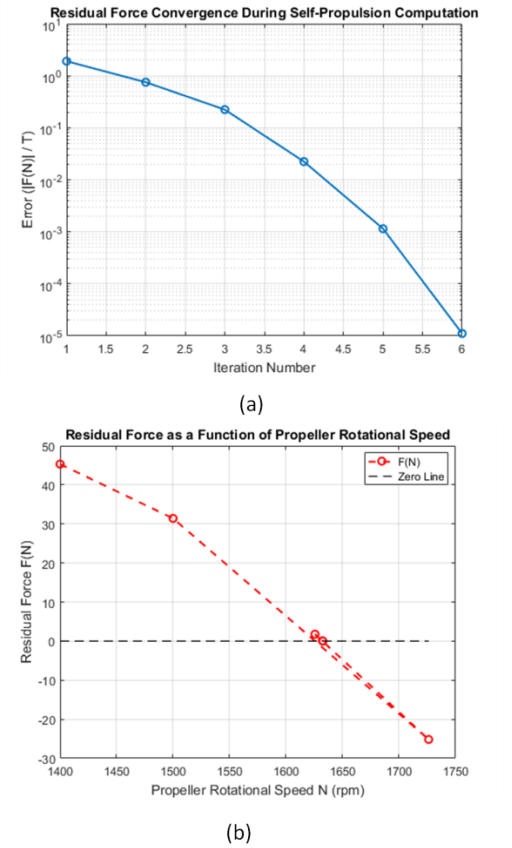

Figure 9. Convergence and residual force behavior during the computation of the self-propulsion condition using the Secant method: (a) Residual force convergence over iterations; (b) Residual force F(N) as a function of propeller rotational speed.

Table 6 displays the propeller thrust alongside the corresponding hydrodynamic resistance forces generated by the hull and rudder at an AUV velocity of 5 m/s. As expected, the hull resistance constitutes the majority of the total resistance, primarily due to its extensive wetted surface area. Approximately 67.5% of the hull resistance is attributed to viscous forces, as demonstrated by the wall shear stress distribution illustrated in Figure 10. Elevated shear stress values are particularly prominent near the bow and along the midsection of the hull. In comparison, the rudder contributes around 21.1% to the total resistance, with pressure forces being the predominant component. This is supported by Figure 11, which shows the static pressure distribution along the AUV's mid-plane and highlights a pronounced pressure gradient between the rudder's leading and trailing edges. This behavior is largely influenced by the geometry of the rudder, which is characterized by a thin profile featuring rounded leading and trailing edges. Figure 12 further illustrates this effect, depicting a relatively smooth flow along the hull surface, in contrast to the significantly disturbed flow observed in the wake region downstream of the rudder.

TABLE 6. PROPELLER THRUST AND THE CORRESPONDING HULL AND RUDDER RESISTANCE FORCES AT AN AUV SPEED OF 5 M/S.

	T	R_hull	R_rudder
Value(N)	81.28	-60.18	-21.10
Pressure Force (%)	104.6%	32.5%	84%
Viscous Force (%)	-4.6%	67.5%	16%

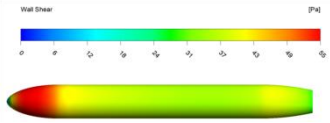

Figure 10. Wall shear stress distribution over the hull surface.

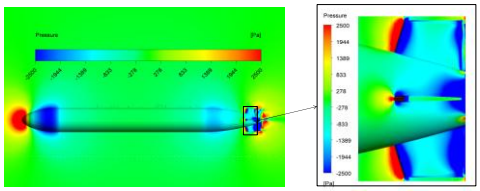

Figure 11. Pressure field around the AUV.

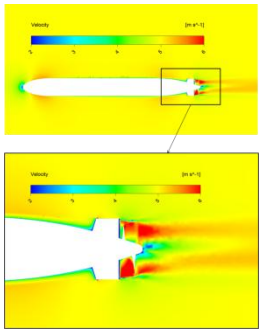

Figure 12. Velocity field around the AUV.

B. AUV in Lateral Current Affected Environment

The second part of this study investigates the behavior of the AUV in an environment influenced by a lateral current, with particular focus on the effects of varying rudder deflection angles and propeller rotational speeds. To achieve this, a series of simulations were conducted using different control configurations, combining various rudder deflection angles and propeller speeds. The objective was to identify the optimal control settings that enable the AUV to sustain a straight and steady trajectory, in accordance with Newton's second law of motion.

Figure 13 presents the net forces acting on the AUV in the x-direction (surge) and y-direction (sway), as well as the net moment around the z-axis (yaw), for various control configurations.

1) Effect of Propeller Rotational Speed on Surge Force

As the propeller's rotational speed increases, it produces increased thrust. This thrust counteracts the hydrodynamic resistance imposed by the hull and rudder, leading to a reduction in the net surge force as illustrated in Figure 13(a).

Thus, an inverse correlation is observed between propeller speed and the net force in the x-direction.

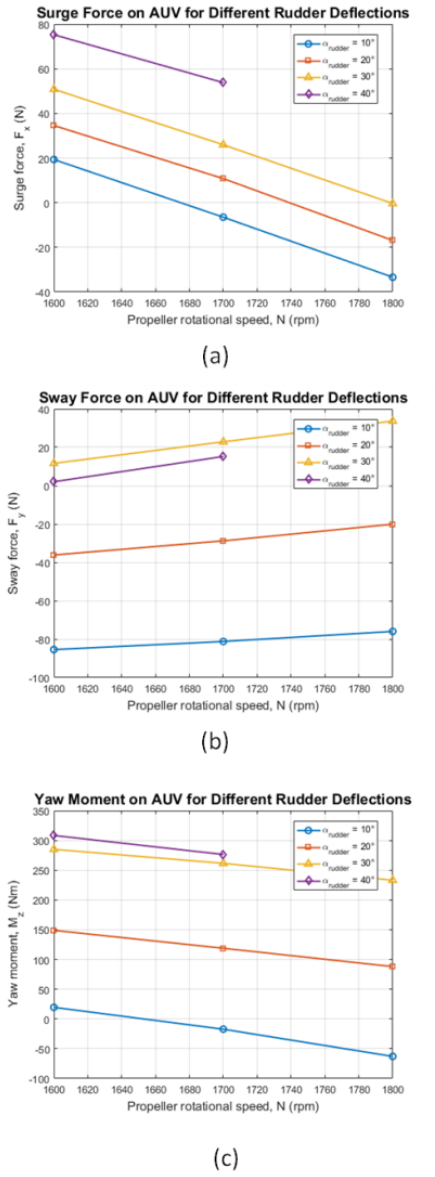

Figure 13. AUV Hydrodynamic Response in (a) Surge, (b) Sway, and (c) Yaw under Varying Control Inputs.

2) *Effect of Rudder Deflection on Surge and Sway Forces*

Increasing the rudder deflection angle amplifies the pressure gradient acting on the rudder blades. This effect is visualized in Figure 14, which shows the pressure field around the rudder at N=1800 rpm for two distinct rudder deflection angles α_{rudder}=20°and α_{rudder} =30°. A clear increase in pressure gradient across the rudder is apparent with increased deflection, leading to enhanced pressure forces induced by the rudder. As a result, both surge and sway forces increase with rudder deflection at a given propeller speed as illustrated in Figure 13(a) and 13(b).

3) *Rudder's Role in Compensating the Yaw Moment*

To counteract the negative yaw moment generated by the hull, the rudder produces a moment in the positive z-direction. This is achieved by deflecting the rudder to generate a pressure-induced moment that opposes the hull's contribution. For the configuration with a rudder deflection angle of α_{rudder} =20° and rotational speed of N=1800 rpm, the rudder contributes up to 99% of the total yaw moment. This dominance of the rudder's pressure force explains the observed increase in net yaw moment with increasing rudder deflection, as illustrated in Figure 13(c).

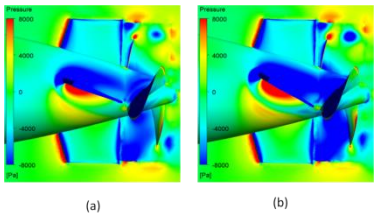

Figure 14. Pressure Field around AUV for N=1800 rpm in Current-Affected Environment: a) α_{rudder}=20°and b) α_{rudder} =30°.

4) *Interaction between Propeller Speed and Rudder-Induced Forces*

For a fixed rudder deflection angle, increasing the propeller rotational speed accelerates the flow around the rudder, consequently amplifying the pressure differential across its surface.

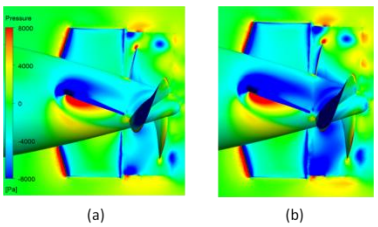

Figure 15. Pressure Field around AUV with α_{rudder}=20°. in Current-Affected Environment: -(a):N=1600 rpm and b) N=1800 rpm

This phenomenon is also depicted in Figure 15, which contrasts the pressure field around the rudder at α_{rudder}=20° for N=1600 rpm and N=1800 rpm. The increased flow velocity at higher propeller speeds results in a more pronounced pressure gradient across the rudder, thereby increasing the sway force.

V. CONCLUSION AND FUTURE WORK

This study presents a simulation-based analysis of the propulsion and stability characteristics of an Autonomous Underwater Vehicle (AUV) during both straight, constant-speed motion and in current-affected environments. The AUV model, consisting of the hull, rudder, and propeller, was simulated under steady-state conditions using the RANS. The CFD methodology was validated against experimental data from open-water propeller tests, showing good agreement with experimental results, thereby confirming the reliability of the adopted numerical approach. A self-propulsion condition was established by coupling CFD with the secant root-finding method to determine the required propeller rotational speed and corresponding thrust to balance the hydrodynamic resistance forces. This method demonstrated high accuracy and robust convergence. Additionally, the behavior of the AUV in a lateral current environment was explored through a series of simulations that varied control inputs—particularly focusing on rudder deflection angles and propeller rotational speeds. The outcomes were analyzed with particular attention to the resulting surge, sway, and yaw responses. Findings reveal a significant interdependence between the control parameters and the hydrodynamic forces and moments, highlighting the importance of precise actuation for maintaining trajectory stability in flow-disturbed environments. As a future direction, this research will be extended through the integration of optimization tools and Artificial Intelligence (AI) algorithms. The goal is to identify optimal control configurations that enable the AUV to effectively navigate complex and dynamic oceanic environments, which include strong marine currents and surface wave disturbances, thus enhancing its operational robustness and mission success.

REFERENCES

[1] R. B. Wynn et al., "Autonomous underwater vehicles (AUVs): their past, present and future contributions to the advancement of marine geoscience," *Marine Geology*, vol. 352, pp. 451–468, Jun. 2014.

[2] K. J. Campbell, S. Kinnear, and A. Thame, "AUV technology for seabed characterization and geohazards assessment," *The Leading Edge*, vol. 34, no. 2, pp. 170–178, 2015.

[3] F.-d. Gao, C.-y. Pan, and Y.-y. Han, "Numerical computation and analysis of unsteady viscous flow around autonomous underwater vehicle with propellers based on sliding mesh," *Journal of Central South University*, vol. 19, pp. 944–952, 2012.

[4] G. Antonelli and E. Cataldi, "Recursive adaptive control for an underwater vehicle carrying a manipulator," in *Proceedings of the 22nd Mediterranean Conference on Control and Automation*, 2014.

[5] T. I. Fossen, *Handbook of Marine Craft Hydrodynamics and Motion Control*. Hoboken, NJ, USA: Wiley, 2011.

[6] A. Honaryar and M. Ghiasi, "Design of a bio-inspired hull shape for an AUV from hydrodynamic stability point of view through experiment and numerical analysis," *Journal of Bionic Engineering*, vol. 15, no. 6, pp. 950–959, 2018.

[7] C. Yu, R. Wang, X. Zhang, and Y. Li, "Experimental and numerical study on underwater radiated noise of AUV," *Ocean Engineering*, vol. 201, p. 107111, 2020.

[8] L. Wu et al., "Hydrodynamic performance of AUV free running pushed by a rotating propeller with physics-based simulations," *Ocean Engineering*, vol. 202, p. 107205, 2020..

[9] Y. Ding, X.-r. Li, Y. Yan, and W.-Q. Wang, "Investigation of the self-propulsion performance of a submarine with a pump-jet propulsor in a surface wave–current coupling environment," *Ocean Engineering*, vol. 298, p. 119306, 2024.

[10] F. Min, G. Pan, and X. Xu, "Modeling of autonomous underwater vehicles with multi-propellers based on maximum likelihood method," *Journal of Marine Science and Engineering*, vol. 8, no. 6, p. 429, 2020.

[11] V. Raja et al., "Multi-domain based computational investigations on advanced unmanned amphibious system for surveillances in international marine borders," *Aerospace*, vol. 9, no. 11, p. 652, 2022.

[12] J. L. D. Dantas and E. A. de Barros, "Numerical analysis of control surface effects on AUV manoeuvrability," *Applied Ocean Research*, vol. 40, pp. 118–126, 2013.

[13] P. Rattanasiri, P. A. Wilson, and A. B. Phillips, "Numerical investigation of a pair of self-propelled AUVs operating in tandem," *Ocean Engineering*, vol. 100, pp. 126–137, 2015.

[14] L. Hong, R. Fang, X. Cai, and X. Wang, "Numerical investigation on hydrodynamic performance of a portable AUV," *Journal of Marine Science and Engineering*, vol. 9, no. 8, p. 812, 2021.

[15] X. Liu, Y. Hu, Z. Mao, W. Ding, and S. Han, "Numerical investigation on interactive hydrodynamic performance of two adjacent unmanned underwater vehicles (UUVs)," *Journal of Marine Science and Engineering*, vol. 11, no. 11, p. 2088, 2023.

[16] W. Tian, B. Song, and H. Ding, "Numerical research on the influence of surface waves on the hydrodynamic performance of an AUV," *Ocean Engineering*, vol. 183, pp. 40–56, 2019.

[17] X. Liu, Y. Hu, Z. Mao, and W. Tian, "Numerical simulation of the hydrodynamic performance and self-propulsion of an UUV near the seabed," *Applied Sciences*, vol. 12, no. 14, p. 6975, 2022.

[18] ANSYS Inc., *ANSYS CFX User's Guide*, Release 18.2, Canonsburg, PA, USA.

[19] T.-H. Joung, K. Sammut, F. He, and S.-K. Lee, "Shape optimization of an autonomous underwater vehicle with a ducted propeller using computational fluid dynamics analysis," *International Journal of Naval Architecture and Ocean Engineering*, vol. 4, pp. 44–56, 2012.

[20] F. Salvatore, F. Pereira, M. Felli, D. Calcagni, and F. Di Felice, *Description of the INSEAN E779A Propeller Experimental Dataset (INSEAN Technical Report No. 2006-085)*. Rome, Italy: INSEAN – Italian Ship Model Basin, 2006.

[21] D. Boucetta and O. Imine, "Numerical simulation of the cavitating flow around marine co-rotating tandem propellers," *Brodogradnja: Shipbuilding*, vol. 70, no. 1, pp. 47–58, 2019.